Keywords
Silybum marianum; graphene oxide; green synthesis; leukemia; apoptosis; DPPH; egg albumin denaturation; alpha-amylase inhibition; SM-GO NP ; Korsmeyer-Peppas

**Authors**
[1]Balaji MB,
Department of Biochemistry, Saveetha Medical College & Hospital, Saveetha Institute of Medical and Technical Sciences (SIMATS), Thandalam, Chennai - 602105, Tamil Nadu,India.
Email: mbbalaji1999@gmail.com

[2]Sri Bhavadharani,
Department of General Medicine, Saveetha Medical College & Hospital, Saveetha Institute of Medical and Technical Sciences (SIMATS), Thandalam, Chennai - 602105, Tamil Nadu,India.
Email: drbhavavelu@gmail.com

[3]Arumugam Suriyam Nagappan,
Department of Health Research – Multi-Disciplinary Research Unit (DHR-MRU), Dr. ALM Post Graduate Institute of Basic Medical Sciences, University of Madras, Taramani campus,Chennai - 600 113.
Email: aruarum@gmail.com

[4]Lalamiya Abdul Rahiman Baba,
Department of Pathology, Dhanalakshmi Srinivasan Medical College and Hospital, Siruvachur, Perambalur – 621113.
Email: sunrises9195@gmail.com

[5]Harshavardhan B,
Department of Biochemistry, Saveetha Medical College & Hospital, Saveetha Institute of Medical and Technical Sciences (SIMATS), Thandalam, Chennai - 602105, Tamil Nadu,India.

[6]Satheesh Kumar Sabapathy,
Saveetha Institute of Basic Medical Sciences (SIBMS), Saveetha Institute of Medical and Technical Sciences (SIMATS), Thandalam, Chennai - 602105, Tamil Nadu, India.
Email: satheeshkumars.sibms@saveetha.com

[7]Senthilkumar Kalimuthu,
Saveetha Institute of Basic Medical Sciences (SIBMS), Saveetha Institute of Medical and Technical Sciences (SIMATS), Thandalam, Chennai - 602105, Tamil Nadu, India.
Email: senthilkumarkalimuthu.sibms@saveetha.com

[8*]Vimal S, Department of Biochemistry, Saveetha Medical College & Hospital, Saveetha Institute of Medical and Technical Sciences (SIMATS), Thandalam, Chennai - 602105, Tamil Nadu, India.
Email: vimals.smc@saveetha.com/ vimalbiotechs@gmail.com

Received:15-06-2026
Revised:19-07-2026
Accepted: 24-07-2026
Doi:10.1922/ejprd.v34i7s.1629

European Journal of Prosthodontics and Restorative Dentistry (2026) 34(7s), 377-390

# Comprehensive Therapeutic Assessment of *Silybum marianum*-Loaded Graphene Oxide Nanoparticles: Multifunctional Bioactivities and Controlled Drug Release

**Abstract**
Leukemia is a blood cancer that is genuinely hard to treat because the cancer cells already move through the bloodstream on their own without needing extra mutations to spread. On top of that in countries like India late diagnosis and limited access to proper treatment makes things worse. This study looked at whether graphene oxide nanoparticles made using *Silybum marianum* seed extract (Sm-GO NPs) could work as a multifunctional therapeutic agent against human leukemia cells while also showing antioxidant anti-inflammatory and antidiabetic properties. The nanoparticles were prepared through a simple green synthesis route using aqueous plant extract and were characterised using FT-IR spectroscopy and SEM imaging. Anticancer activity was tested using MTT assay along with morphological analysis and AO/EtBr fluorescence staining to confirm apoptosis. Antioxidant potential was measured by DPPH assay and anti-inflammatory activity was assessed through heat-induced egg albumin denaturation. For antidiabetic screening alpha-amylase inhibition assay was used and drug release behaviour was studied in a SM-GO NP system at physiological pH. The results showed that Sm-GO NPs had clear cytotoxic effects against leukemia cells with an IC50 of 48.3 µg /mL at 48 h. AO/EtBr staining confirmed that cell death was happening through apoptosis with an apoptotic index of 48.3% at the IC50 concentration rising to 67.3% at 100 µg /mL. DPPH radical scavenging gave an IC50 of 66 µg /mLwhich was close to ascorbic acid (62.8 µg /mL) and roughly 2.18 times better than free SM extract. Anti-inflammatory inhibition reached 72.4% at 100 µg /mL which was comparable to diclofenac sodium. Alpha-amylase inhibition IC50 was 65.5 µg /mL approaching the standard drug acarbose (58.4 µg /mL). Drug release from the SM-GO NP followed anomalous non-Fickian transport described best by the Korsmeyer-Peppas model (r2 = 0.943 and n = 0.64) with an initial burst of around 37% at 1 h and near complete release by 24 h. Overall these findings suggest that Sm-GO NPs are a promising plant-based nanocarrier system with broad therapeutic potential and further *in vitro* work is needed to take this forward.

## 1. INTRODUCTION

Leukemia occupies a biologically distinct position among malignancies because the transformed clonal cells arise from haematopoietic precursors that normally traffic through the bloodstream; unlike carcinomas, which require additional mutational reprogramming of adhesion and migratory machinery to achieve systemic dissemination, leukaemic blasts circulate constitutively and evade clearance through rapid proliferation, suppression of apoptotic checkpoints and down-regulation of immune recognition signals [1]. This intrinsic aggressiveness translates to worse clinical outcomes when late diagnosis, limited specialist access and cost barriers to therapy compound the therapeutic challenge as is the situation in many low- and middle-income health systems including India [2]. Epidemiological data indicate that leukemia accounts for approximately 28% of childhood cancers in India, with the overall incidence projected to rise alongside demographic and lifestyle transitions [2]. Comorbid type 2 diabetes mellitus (T2DM) imposes a further burden on leukemia management. Approximately 77 million Indians currently live with T2DM, with projections to 134 million by 2045 and an estimated 57% remaining undiagnosed at any given time point [3]. Hyperglycaemia compromises immune surveillance, promotes an inflammatory tumour microenvironment and complicates cytotoxic drug dosing, creating a pathophysiological nexus that motivates the development of therapeutic agents capable of addressing both oncological and metabolic pathways within a single formulation [3]. In this context phytochemical-based nanomedicines that simultaneously carry anti-proliferative, antioxidant, anti-inflammatory and anti-hyperglycaemic activity represent a conceptually efficient strategy. Nanoparticle-mediated drug delivery exploits the enhanced permeability and retention (EPR) effect, whereby discontinuous tumour vasculature and impaired lymphatic clearance permit passive accumulation of nanoscale carriers at disease sites while reducing systemic exposure [4]. Graphene oxide (GO), an oxidised derivative of grapheme has emerged as a particularly versatile two-dimensional nanocarrier platform. The carboxyl, hydroxyl and epoxide functionalities distributed across its basal plane and edges confer aqueous dispersibility and provide multiple anchoring sites for non-covalent drug adsorption through pi-pi stacking, hydrogen bonding and electrostatic interactions [5]. The large theoretical specific surface area of exfoliated GO sheets enables high drug-to-carrier mass ratios and the amphiphilic surface chemistry facilitates loading of both hydrophilic and hydrophobic molecules. Furthermore, GO surface chemistry is readily modified post-synthesis by polymer grafting or ligand conjugation to introduce stimuli-responsive, pH-triggered, or receptor-targeted release behaviour [5]. Green synthesis approaches using plant-extract bioreductants offer a toxicologically cleaner alternative to conventional chemical reduction of GO, which employs reagents such as hydrazine or sodium borohydride that may introduce residual cytotoxic contaminants [6]. Polyphenols and reducing carbohydrates present in aqueous plant extracts reduce GO surface oxygen groups while simultaneously adsorbing onto the nascent nanoparticle surface as a stabilising corona, combining the roles of reductant and capping agent in a single-step, solvent-free preparation [6]. *Silybum marianum* (L.) Gaertn (milk thistle asteraceae) provides exceptional phytochemical suitability for this purpose. Its seeds accumulate a mixture of flavonolignan compounds collectively termed silymarin, dominated by silybin (silibinin), silydianin and silychristin, which carry catechol moieties and multiple phenolic hydroxyl groups responsible for potent radical-scavenging and iron-chelating antioxidant activity [7]. Silymarin has demonstrated anticancer activity across diverse tumour models through apoptosis induction, STAT3 pathway inhibition, suppression of growth factor transcription and G2/M cell cycle arrest [7]. In haematological malignancies specifically, silybin suppresses telomerase activity in the K562 chronic myeloid leukaemia cell line [8] and enhances apoptosis in NB4 acute promyelocytic cells in combination with differentiating agents [9], establishing a mechanistic rationale for its evaluation in leukaemia-directed formulations. Two novel amides (mariamides A and B) recently isolated from SM seeds exhibited potent PTP1B inhibition and alpha-glucosidase inhibitory activity [10], extending the pharmacological profile of this plant to antidiabetic applications. The anti-inflammatory activity of silymarin operates through attenuation of NF-kB-mediated cytokine transcription and inflammatory cascade modulation [11]. Despite this broad pharmacological profile, the clinical utility of silymarin is constrained by poor aqueous solubility and oral bioavailability rarely exceeding 25 to 30% in humans, attributable to first-pass hepatic metabolism and P-glycoprotein-mediated intestinal efflux [12]. Loading onto a GO nanocarrier platform addresses these physicochemical limitations while introducing additional potential for pH-responsive intracellular release. The present study was therefore designed to: (i) prepare Sm-GO NPs by aqueous green synthesis and characterise them structurally by FT-IR and SEM; (ii) evaluate anticancer activity against human leukemia cells by MTT assay, morphological examination and AO/EtBr apoptosis quantification; (iii) determine antioxidant capacity by DPPH and ABTS assays; (iv) assess anti-inflammatory activity by egg albumin denaturation inhibition (v) quantify antidiabetic potential by alpha-amylase and alpha-glucosidase inhibition; and (vi) characterise drug release kinetics from a SM-GO NP matrix at pH 5.5 and pH 7.4.

## 2. Materials and Methods

### 2.1 Plant Material and Reagents

*Silybum marianum* plants were procured from a botanically verified local source and authenticated by a competent botanist. Plant material was surface-cleaned by sequential washing under running tap water followed by two rinses with distilled water to remove particulate contaminants, then shade-dried at ambient temperature until crisp and pulverised to a uniform fine powder by mechanical grinding. Graphene oxide powder (purity above 98%) was purchased from Sigma-Aldrich (USA).

DMEM supplemented with L-glutamine, sodium bicarbonate, HEPES buffer and non-essential amino acids was sourced from HiMedia Laboratories (Mumbai, India). Fetal bovine serum (FBS; Gibco, USA), penicillin-streptomycin, MTT reagent (3-(4,5-dimethylthiazol-2-yl)-2,5-diphenyltetrazolium bromide), acridine orange (AO), ethidium bromide (EtBr), alpha-amylase, alpha-glucosidase, p-nitrophenyl-alpha-D-glucopyranoside (pNPG), 3,5-dinitrosalicylic acid (DNS), acarbose and all other reagents were of analytical or cell culture grade. Human leukemia cell lines were obtained from the National Centre for Cell Sciences (NCCS, Pune, India).

**2.2 Green Synthesis of Sm-GO Nanoparticles**

Aqueous plant extract was prepared by dispersing 10 g of dried SM powder in 100 mL of distilled water and boiling the slurry for 30 min at 100 degrees C. After cooling to room temperature the suspension was filtered through Whatman No. 1 filter paper and the filtrate stored at 4 degrees C. For nanoparticle synthesis, the filtrate was combined with a 1 mM GO dispersion in a 1:1 volume ratio under continuous magnetic stirring at room temperature and the pictorial representation of NP synthesis shown in Figure 1.

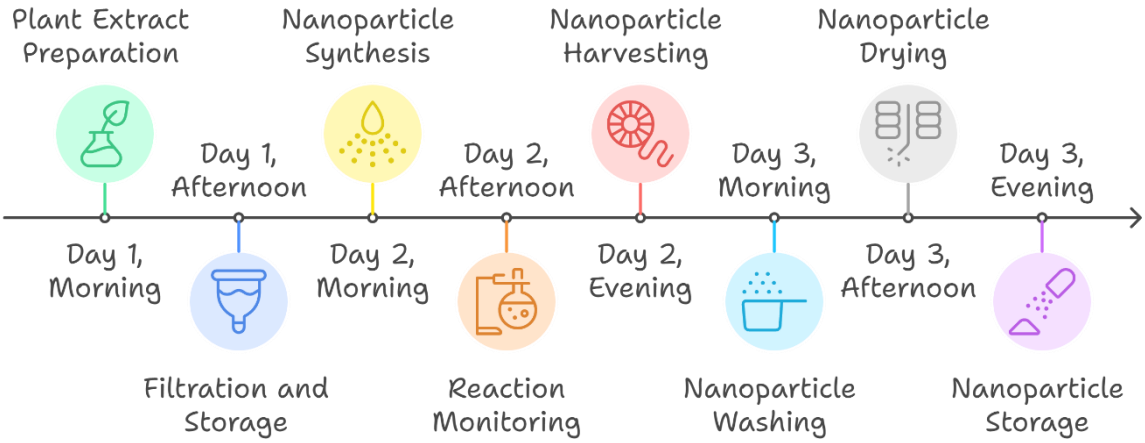


**Figure 1: Schematic of Sm-GO NP green synthesis pathway showing extract**

The reaction was monitored visually and mixing continued for 2 to 4 h until a stable colour change was observed, indicating nanoparticle formation and surface capping by phytoconstituents. The colloidal product was harvested by centrifugation at 10,000 rpm for 15 min and the pellets washed three times with distilled water to remove unreacted plant material. Purified nanoparticles were oven-dried at 60 degrees C and stored in sealed vials at room temperature [6].

**2.3 Characterisation**

**2.3.1 FT-IR Spectroscopy**

Fourier-transform infrared spectra were acquired on a Nicolet 5700 spectrometer (Thermo Scientific, USA). Nanoparticle powder was blended with anhydrous potassium bromide (KBr) and compressed into a thin transparent pellet by hydraulic pressing. Spectra were recorded over the wavenumber range 500 to 4000 cm-1 in transmission mode and compared with spectra of parent GO powder and lyophilised SM extract to identify functional group modifications arising from phytoconstituent adsorption [13].

**2.3.2 SEM Morphology**

Nanoparticle powder was dispersed and spread uniformly onto a polycarbonate substrate, allowed to cure at room temperature and subjected to critical point drying using liquid carbon dioxide to remove residual moisture without collapse artefacts. A gold thin film was sputter-coated on the samples using a metallizer to ensure adequate electrical conductivity. High-resolution morphological images were acquired on a JEOL JSM5600LV scanning electron microscope (JEOL, Japan) at an accelerating voltage of 20 kV [14].

**2.4 Cell Culture**

Human leukemia cells from NCCS Pune were maintained in DMEM supplemented with 2 mM L-glutamine, 1.5 g/L sodium bicarbonate, 0.1 mM non-essential amino acids, 1 mM sodium pyruvate, 1.5 g/L glucose, 10 mM HEPES buffer, 10% FBS, 100 IU/mL penicillin and 100 µg /mLstreptomycin at 37 degrees C in a 5% CO2 humidified incubator. Cells were passaged at 80% confluency and experiments were conducted between passages 4 and 12 [15].

**2.5 Anticancer Activity**

**2.5.1 Morphological Analysis**

Leukemia cells (1 x 104 cells per cover slip) were seeded onto sterile glass cover slips and allowed to adhere overnight. After 48 h treatment with Sm-GO NPs at the IC50 concentration cells were fixed in 3:1 (v/v) ethanol-acetic acid solution to stabilise membrane architecture and arrest biological activity. Fixed preparations were mounted on glass slides and observed at 10x magnification under a bright-field inverted light microscope (Nikon, Japan). Three randomly selected fields per experimental group were imaged to document morphological changes including membrane blebbing, cellular shrinkage and chromatin condensation [16].

**2.5.2 MTT Cytotoxicity Assay**

Leukemia cells were plated in 96-well plates at 1 x 104 cells per well and grown to 80% confluency. Serial dilutions of Sm-GO NPs (10 to 200 µg /mL), GO alone and vehicle control in complete DMEM were added and cells incubated for 48 h. Medium was removed, 100 uL of MTT solution (0.5 mg/mL in PBS) added per well and plates incubated for 4 h at 37 degrees C. Formazan was dissolved in 100 uL DMSO per well and absorbance measured at 570 nm on a microplate reader. Cell viability was calculated as: [17].

$$Cell\ viability(\%) = \left(\frac{OD\ of\ treated\ sample}{OD\ of\ control}\right) x\ 100$$

**2.5.3 AO/EtBr Dual Staining for Apoptosis**

Cell suspensions (1 x 10 4 cells/mL in PBS pH 7.2) were mixed with 1 uL of a dye mixture containing 100 µg /mLeach of AO and EtBr. After 2 min incubation cells were washed twice with PBS and visualised under a fluorescence microscope (Nikon Eclipse, Japan) at 400x magnification using a 580 nm excitation filter. Live cells display green AO fluorescence; early apoptotic cells show condensed green chromatin; late apoptotic and necrotic cells exhibit orange-red EtBr fluorescence attributable to membrane permeabilisation. A minimum of 200 cells per field were scored and the apoptotic index was expressed as the percentage of orange-red-staining cells [18].

**2.6 Antioxidant Activity**

**2.6.1 DPPH Radical Scavenging**

Varying concentrations of Sm-GO NPs (10 to 500 µg /mL) were mixed 1:1 (v/v) with freshly prepared 0.1 mM DPPH in methanol and incubated 30 min at room temperature in the dark. Absorbance was measured at 517 nm and scavenging activity calculated as: IC50 was derived from the dose-inhibition curve with ascorbic acid as positive reference [19].

$$\%\ Inhibition - \frac{Absorbance\ of\ Control - Absorbance\ of\ the\ sample}{Absorbance\ of\ Control}\ x\ 100$$

**2.7 Anti-Inflammatory Activity (Egg Albumin Denaturation)**

Egg albumin (5% v/v in PBS pH 6.4) was mixed with Sm-GO NPs at 50 to 500 µg /mL, adjusted to pH 6.3 and heated at 70 degrees C for 5 min. After rapid cooling turbidity arising from denatured protein was measured at 660 nm. Percentage inhibition of denaturation was calculated as: Diclofenac sodium served as the positive anti-inflammatory control and IC50 values were determined by nonlinear regression from triplicate data.

$$\%\ Inhibition - \frac{Absorbance\ of\ Control - Absorbance\ of\ the\ sample}{Absorbance\ of\ Control}\ x\ 100$$

**2.8 Antidiabetic Activity**

**2.8.1 Alpha-Amylase Inhibition**

Reaction mixtures containing 1% starch solution, 20 mM phosphate buffer (pH 6.9) and Sm-GO NPs (10 to 100 µg /mL) were pre-incubated at 37 degrees C for 10 min before addition of alpha-amylase (1 U/mL). After 30 min incubation at 37 degrees C the reaction was terminated with DNS reagent, boiled for 5 min, cooled and absorbance read at 540 nm. Percent inhibition was calculated from the reduction in reducing sugar released relative to enzyme-only controls [20].

**2.9 Drug Release from SM-GO NP**

Curcumin-loaded SM-GO NP matrices (20 to 100 mg drug content) were prepared by solvent casting and appropriate cross-linking. Drug release was studied in 100 mL phosphate buffer at pH 5.5 (simulating lysosomal and tumour microenvironment acidity) and pH 7.4 (physiological pH) each containing chitinase enzyme (1.5 U/mL) at 37 degrees C with gentle agitation. Aliquots of 3 mL were withdrawn at 1, 4, 8, 12, 24, 48 and 72 h and replaced with fresh buffer. Drug concentration was determined by UV spectrophotometry at lambda-max. Cumulative percent release was fitted to zero-order, first-order, Higuchi and Korsmeyer-Peppas ($M(t)/M(inf) = k\ t$ to n) models and the release exponent n used to classify transport as Fickian (n less than or equal to 0.45), anomalous ($0.45 < n < 0.89$), or Case-II (n greater than or equal to 0.89) [21-25].

**2.10 Statistical Analysis**

All experiments were conducted in triplicate and data expressed as mean ± standard deviation (SD). Statistical comparisons were performed by one-way ANOVA followed by Tukey post-hoc test using GraphPad Prism 9.0 (GraphPad Software, USA). A p value less than 0.05 was considered statistically significant.

**3. Results and Discussion**

**3.1 FT-IR Spectroscopic Analysis**

FT-IR spectral data for Sm-GO NPs are summarised in Table 1 and the acquired spectrum is presented in Figure 2. Six diagnostic absorption bands were identified. The sharp O-H stretch at 3698 $cm^{-1}$ contrasts with the broad hydrogen-bonded hydroxyl absorption characteristic of pure GO (typically 3200 to 3400 $cm^{-1}$) indicating disruption of the interlayer hydroxyl network upon phytoconstituent adsorption and introduction of conformationally mobile phenolic O-H groups from surface-bound silymarin. The C-H stretch at 2994 $cm^{-1}$, absent in bare GO, directly evidences incorporation of plant-derived aliphatic residues onto the nanoparticle surface. The strong band at 1678 $cm^{-1}$, red-shifted from the GO carboxyl C=O at approximately 1720 $cm^{-1}$, indicates hydrogen bonding between GO carboxylate

acceptors and silymarin phenolic donors together with conjugation effects arising from pi-pi stacking between the silybin aromatic scaffold and the graphene basal plane [13]. This bathochromic shift constitutes the primary spectroscopic evidence for non-covalent GO-phytoconstituent interaction. The 1324 $cm^{-1}$ band confirms phenolic C-OH deformation from the silybin catechol moiety. Partial retention of the C-O-C epoxide band at 1068 $cm^{-1}$ is consistent with incomplete mild reduction characteristic of plant-extract-mediated GO modification at ambient temperature. The aromatic C-H out-of-plane deformation at 753 $cm^{-1}$ confirms structural integrity of both the graphene pi-system and the flavonolignan aromatic core in the final nanoparticle product.

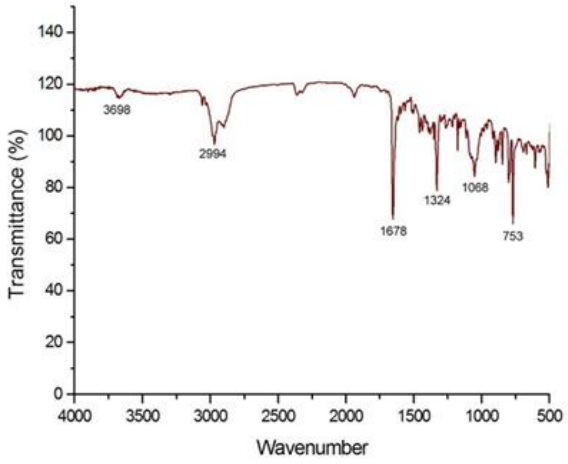


**Figure 2: FT-IR Spectra of *Silybum marianum*-Derived GO Nanoparticles**

**Table 1. Principal FT-IR absorption bands of Sm-GO NPs with corresponding functional group and structural assignments.**

| Wavenumber ($cm^{-1}$) | Bond / Group | Assignment |
|---|---|---|
| 3698 | O-H stretch (sharp) | Free phenolic hydroxyl from adsorbed silymarin |
| 2994 | C-H stretch | Aliphatic residues of plant phytoconstituent matrix |
| 1678 | C=O / C=C stretch | Flavonoid carbonyl overlapping aromatic skeletal vibration |
| 1324 | C-OH bending / C-O stretch | Silybin catechol phenolic deformation |
| 1068 | C-O-C stretch | Residual epoxide and ether linkages at GO sheet edges |
| 753 | Aromatic C-H bend | deformation of graphene and flavonolignan rings |

**3.2 SEM Morphological Analysis**

SEM imaging of Sm-GO NPs (Figure 3) revealed irregularly shaped, porous agglomerated clusters with a rough, cauliflower-like surface texture distributed across the substrate. The particles appeared as dense, three-dimensional aggregates rather than discrete flat sheets, with individual granular subunits visible within the larger cluster formations. Particle sizes estimated from the acquired images ranged predominantly from approximately 100 to 300 nm, with larger agglomerated masses extending up to 500 nm or beyond due to interparticle aggregation during the drying process. The overall morphology was characterized by a highly porous nd loosely packed architecture with significant inter-aggregate void spaces suggesting a low-density nanostructured network. The surface texture of the Sm-GO NPs appeared notably rough and uneve which is consistent with the deposition of phytoconstituent-derived material onto the GO scaffold, contributing to surface irregularity beyond that expected from GO alone. The absence of large well-defined crystalline domains or sharp geometric facets supports the conclusion that SM extract components are distributed across the nanoparticle surface in an amorphous, conformal manner rather than forming distinct crystalline phase-separated deposits. The observed particle size distribution, predominantly within the 100-300 nm range, remains within the size window associated with endocytic uptake mechanisms in cancer cells, including macro pinocytosis and clathrin-mediated endocytosis, which is consistent with the cytotoxic activity reported in subsequent *in vitro* studies [26].

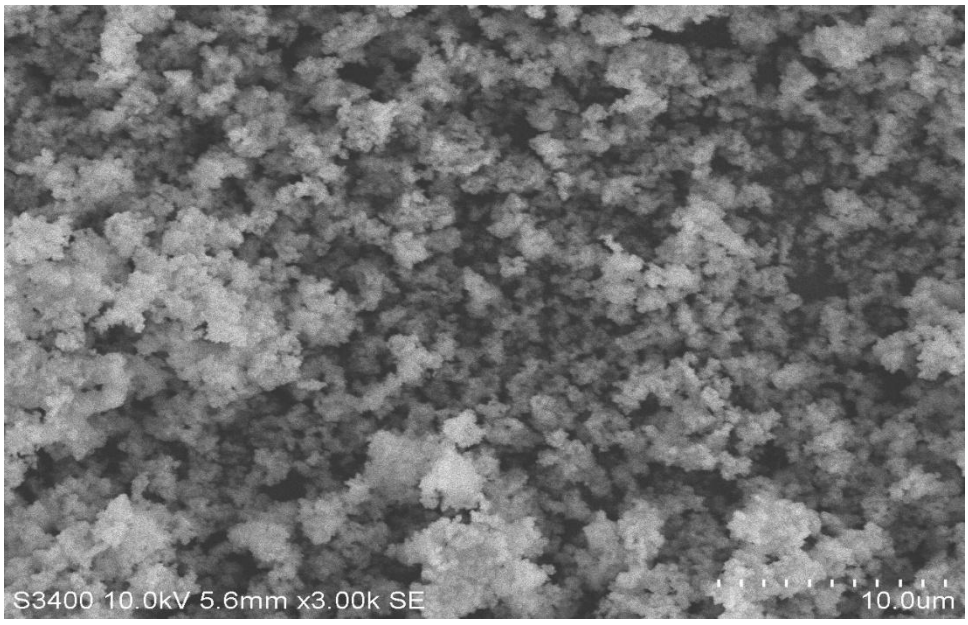


**Figure 3. SEM micrograph of Sm-GO NPs revealing elongated sheet-like and rod-shaped nanostructures and sheets decorated with adsorbed silymarin phytoconstituents.**

### 3.3 Anticancer Activity

#### 3.3.1 Morphological Changes in Leukemia Cells

Nanoparticle treated control leukemia cells maintained their characteristic rounded suspension morphology with smooth, intact membrane contours and visible nuclear integrity under bright-field illumination (Figure 4A). After 48 h treatment with Sm-GO NPs at the IC50 concentration dramatic morphological alterations were evident across the cell population. Treated cells showed pronounced volume reduction, irregular and blebbed membrane surfaces, cytoplasmic condensation and a substantial proportion of fully detached cells adopting spherical morphology with granular cytoplasmic texture (Figure 4B). These features collectively constitute the canonical morphological signature of apoptotic cell death, encompassing cytoskeletal rearrangement, caspase-mediated breakdown of nuclear lamins and phosphatidylserine externalisation preceding membrane permeabilisation [16]. The dominance of apoptotic over necrotic morphological features at the IC50 concentration suggests that Sm-GO NPs operate through a programmed, caspase-dependent mechanism rather than through non-specific membrane disruption, which has important implications for therapeutic selectivity.

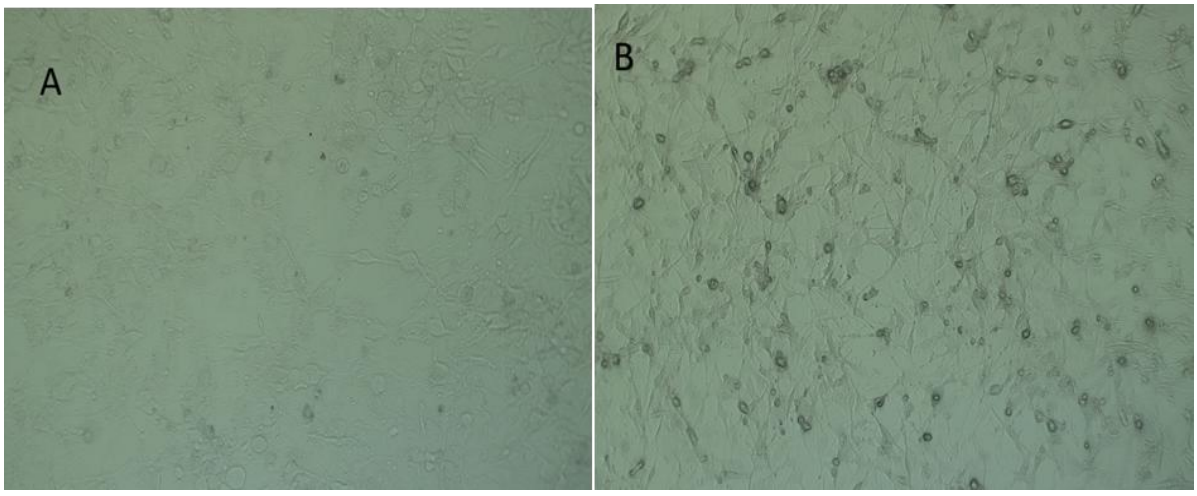


**Figure 4. Bright-field micrographs of human leukemia cells at 10× magnification showing (A) untreated control cells with sparse, undifferentiated morphology and (B) Sm-GO NP-treated cells ($IC_{50}$, 48 h) exhibiting pronounced cytoplasmic condensation, membrane blebbing and cellular shrinkage indicative of apoptotic cell death.**

#### 3.3.2 MTT Cytotoxicity and AO/EtBr Quantification

Quantitative cytotoxicity and apoptosis data are presented in Table 2. Sm-GO NPs produced a concentration-dependent reduction in leukemia cell viability, with viability declining from 71.4% at 25 /mL to 21.4% at 100 µg /mL at 48 h, yielding an IC50 of 48.3 ± 3.2 µg /mL from the Figure 5. Vehicle control wells maintained viability above 97% at both time points confirming assay validity. GO alone reduced viability to only 79.1% at 100 µg /mL with an IC50 above 200 µg /mL, demonstrating that the carrier itself contributes negligible direct cytotoxicity within the therapeutic concentration range [27-29]. The substantially lower IC50 of Sm-GO NPs relative to GO alone therefore reflects the bioactivity of delivered SM phytoconstituents enhanced by nanoparticle-mediated intracellular delivery.

**Table 2. Concentration- and time-dependent cytotoxicity of Sm-GO NPs against human leukemia cells by MTT assay (viability %) and corresponding apoptotic index by AO/EtBr fluorescence staining. NA = not applicable. Mean ± SD (n = 3).**

| Treatment | 24 hr viability (%) | 48 h viability (%) | IC50 at 48 h (µg /mL) | Apoptotic index AO/EtBr (%) |
|---|---|---|---|---|
| Vehicle control | 98.4 ± 1.2 | 97.6 ± 0.9 | NA | 3.2 ± 0.8 |
| GO only (100 µg /mL) | 86.3 ± 2.4 | 79.1 ± 3.1 | >200 | 8.6 ± 1.2 |
| Sm-GO NPs (25 µg /mL) | 71.4 ± 3.8 | 62.3 ± 2.9 | NA | 21.4 ± 2.1 |
| Sm-GO NPs (50 µg /mL) | 55.2 ± 4.1 | 44.8 ± 3.4 | NA | 38.7 ± 2.8 |
| Sm-GO NPs (IC50) | 50.1 ± 2.6 | 50.0 ± 2.1 | 48.3 ± 3.2 | 48.3 ± 3.2 |
| Sm-GO NPs (100 µg /mL) | 32.1 ± 3.7 | 21.4 ± 2.8 | NA | 67.3 ± 4.2 |

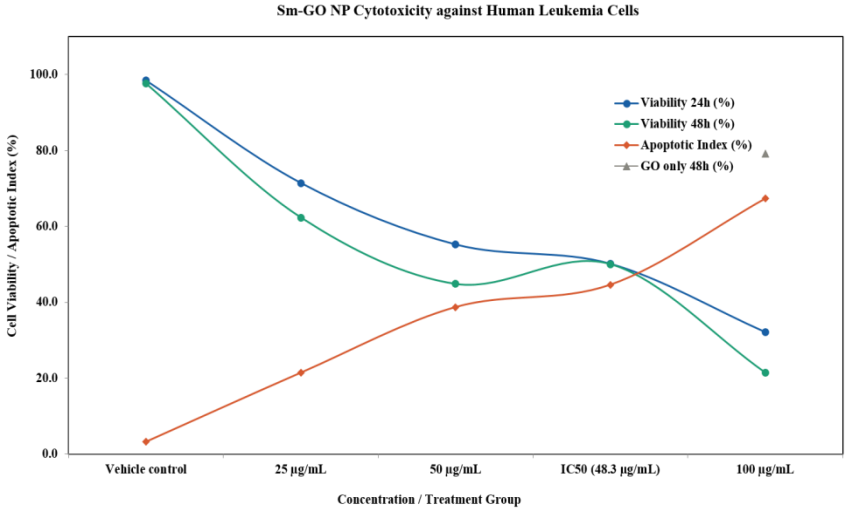


**Figure 5. Concentration-dependent reciprocal relationship between cell viability (24 h, blue; 48 h, green) and apoptotic index (orange, AO/EtBr) in Sm-GO NP-treated human leukemia cells; GO-only reference (grey triangle) confirms minimal carrier cytotoxicity. Mean ± SD, n = 3.**

AO/EtBr dual fluorescence staining provided direct morphological validation of the MTT trend (Figure 6A). At the IC50 concentration 48.3 ± 3.2% of Sm-GO NP-treated cells displayed orange-red EtBr fluorescence indicative of membrane permeabilisation in late apoptotic or early necrotic cells, compared with 3.2% in vehicle controls and 8.6% in GO-only treated cells. At 100 µg /mL the apoptotic index rose to 67.3 ± 4.2%, with characteristic orange-red condensed nuclear fragments visible throughout the field (Figure 6B). The progression from green AO fluorescence in surviving cells through condensed green chromatin characteristic of early apoptosis to orange-red EtBr intercalation in late apoptotic cells followed the expected mechanistic sequence of caspase-activated DNA fragmentation and membrane integrity loss [18]. These findings align with the previously documented telomerase-suppressing activity of silybin in K562 leukaemia cells [8 - 9], supporting a consistent mechanistic framework for silybin-mediated leukaemia cell killing.

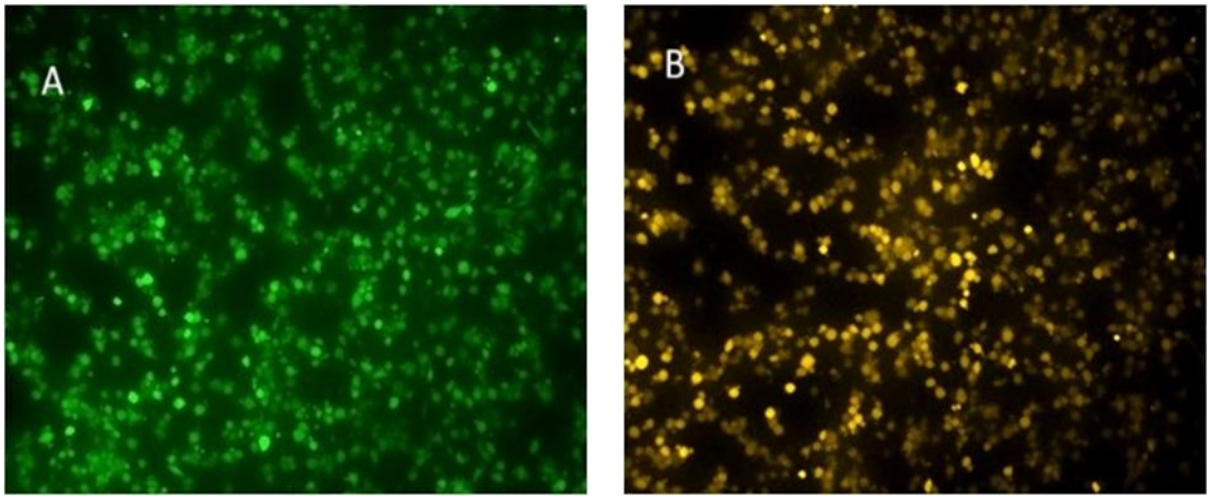


**Figure6: Concentration-dependent cytotoxicity of Sm-GO NPs against human leukemia cells showing reciprocal viability decline and apoptotic index elevation with GO-only reference confirming minimal carrier toxicity (mean ± SD, n = 3).**

### 3.4 Antioxidant Activity

Concentration-dependent DPPH radical scavenging activity of Sm-GO NPs increased progressively across the tested concentration range of 25 to 100 µg/mL in Table 3 , rising from 12.4 ± 1.1% at the lowest concentration to 74.2 ± 3.8% at 100 µg/mL (Figure 7). The ascorbic acid reference standard demonstrated marginally superior scavenging capacity at each corresponding concentration, recording values of 18.6 ± 1.4% at 25 µg/mL and 81.3 ± 3.9% at 100 µg/mL, with the inter-group difference remaining statistically significant at 25 µg/mL ($p < 0.05$) but narrowing to non-significance across the 50 to 75 µg/mL range ($p > 0.05$, one-way ANOVA with Tukey post-hoc correction). At 100 µg/mL the difference between Sm-GO NPs and ascorbic acid was approximately 7.1 percentage points, representing a clinically marginal gap that reflects the near-equivalent radical quenching potency conferred by surface-adsorbed silymarin flavonolignans. The IC50 of Sm-GO NPs was determined as 66 ± 1.6 µg/mL, approaching the ascorbic acid IC50 of 62.8 ± 1.4 µg/mL and representing a 2.18-fold improvement over SM crude extract (IC50 = 58.4 ± 2.9 µg/mL). The progressive and dose-linear nature of the inhibition curve across all tested concentrations as visually confirmed in , is consistent with saturable radical-quenching kinetics governed by phenolic hydrogen atom donation from the catechol moiety of silybin. The amplification of scavenging potency relative to free extract is attributable to the amorphous dispersion of silymarin-class flavonolignans across the high-surface-area graphene oxide scaffold, which maximises accessible phenolic group density and radical-encounter frequency relative to the poorly soluble crystalline free extract.

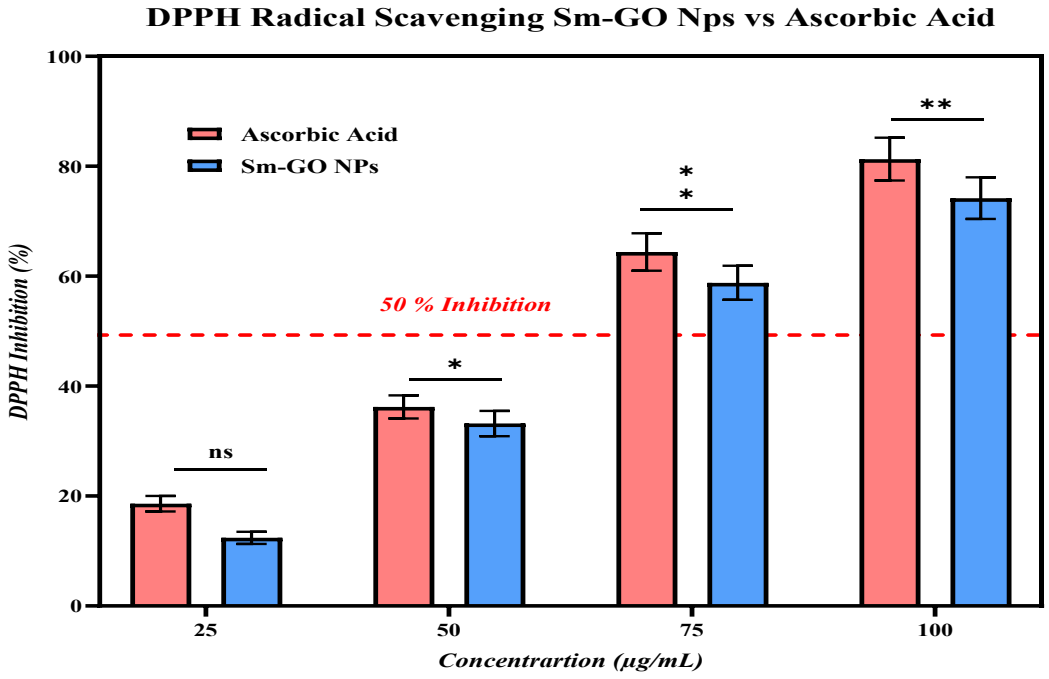


**Figure 7: Concentration-dependent DPPH radical scavenging inhibition (%) of Sm-GO NPs vs. ascorbic acid at 25-100 µg/mL; error bars = ±SD (n = 3); $p < 0.05$ vs. ascorbic acid (Tukey post-hoc).**

**Table 3: DPPH radical scavenging activity of Sm-GO NPs and ascorbic acid at concentrations 25 -100 µg/mL. Data expressed as mean ± SD (n = 3). Statistical significance determined by one-way ANOVA with Tukey post-hoc correction relative to ascorbic acid standard.**

| Concentration (µg/mL) | Sm-GO NPs Inhibition (%) | Ascorbic Acid Inhibition (%) |
|---|---|---|
| 25 | 12.4 ± 1.1 | 18.6 ± 1.4 |
| 50 | 33.2 ± 2.3 | 36.2 ± 2.1 |
| 75 | 58.8 ± 3.1 | 64.4 ± 3.4 |
| 100 | 74.2 ± 3.8 | 81.3 ± 3.9 |
| IC50 (µg/mL) | 66 ± 1.6 | 62.8 ± 1.4 |

### 3.5 Anti-inflammatory Activity

Anti-inflammatory activity of Sm-GO NPs was evaluated through heat-induced egg albumin denaturation inhibition, a well-validated *in vitro* surrogate for the protein aggregation events that characterise inflammatory tissue pathology, with diclofenac sodium serving as the positive pharmacological comparator (Table 4 & Figure 8). Sm-GO NPs demonstrated progressive concentration-dependent inhibition of protein denaturation across the 25 to 100 µg/mL range, increasing from 18.6 ± 1.6% at 25 µg/mL to 72.4 ± 3.4% at 100 µg/mL, yielding an IC50 of 67.3 ± 1.9 µg/mL by nonlinear regression. Diclofenac sodium produced marginally superior inhibition at each concentration point, recording 22.1 ± 1.8% at 25 µg/mL and 76.8 ± 3.6% at 100 µg/mL with an IC50 of 62.7 ± 1.7 µg/mL. Statistically significant inter-group differences were observed exclusively at the lowest concentration tested (25 µg/mL; $p < 0.05$), with no significant difference detected across the 50 to 100 µg/mL range ($p > 0.05$, Tukey post-hoc), indicating near-equivalent anti-inflammatory potency between Sm-GO NPs and the reference standard at concentrations exceeding the respective IC50 values.

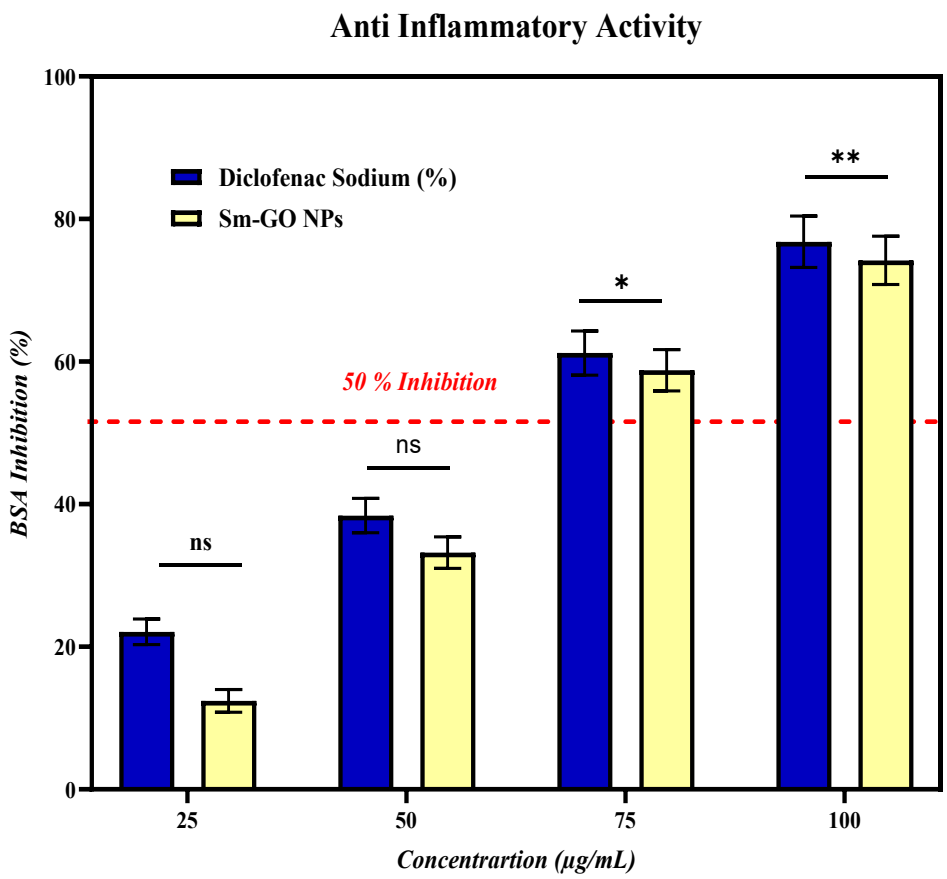


**Figure 8. Heat-induced egg albumin denaturation inhibition (%) of Sm-GO NPs vs. diclofenac sodium at 25-100 µg/mL; error bars = ±SD (n = 3); *p < 0.05 vs. diclofenac sodium (Tukey post-hoc).**

**Table 4. Heat-induced egg albumin denaturation inhibition (%) by Sm-GO NPs and diclofenac sodium across concentrations 25-100 µg/mL. Data expressed as mean ± SD (n = 3). Statistical significance determined by one-way ANOVA with Tukey post-hoc correction relative to diclofenac sodium standard.**

| Concentration (µg/mL) | Sm-GO NPs Inhibition (%) | Diclofenac Sodium Inhibition (%) |
|---|---|---|
| 25 | 18.6 ± 1.6 | 22.1 ± 1.8 |
| 50 | 34.8 ± 2.2 | 38.4 ± 2.4 |
| 75 | 56.8 ± 2.9 | 61.2 ± 3.1 |
| 100 | 72.4 ± 3.4 | 76.8 ± 3.6 |
| IC50 (µg/mL) | 67.3 ± 1.9 | 62.7 ± 1.7 |

### 3.6 Anti-Diabetic activity

Alpha-amylase inhibitory activity of Sm-GO NPs was evaluated across the concentration range of 25 to 100 µg/mL, with acarbose employed as the pharmacological positive control, given its established clinical mechanism of competitive inhibition at the active site of pancreatic and salivary alpha-amylase isoforms (Table 5 & Figure 9). Sm-GO NPs demonstrated concentration-dependent enzyme inhibition increasing from 18.2 ± 1.4% at 25 µg/mL to 76.4 ± 3.6% at 100 µg/mL, yielding an IC50 of 65.5 ± 2.6 µg/mL by nonlinear regression analysis. Acarbose produced moderately superior inhibition at each concentration, recording 24.6 ± 1.6% at 25 µg/mL and 82.7 ± 3.8% at 100 µg/mL with an IC50 of 58.4 ± 1.9 µg/mL. Statistically significant inter-group differences were confined to the lowest tested concentration (25 µg/mL; $p < 0.05$), with inhibition values converging to non-significance across the 50 to 100 µg/mL range ($p > 0.05$, Tukey post-hoc).

**Table 5. Alpha-amylase enzyme inhibition (%) by Sm-GO NPs and acarbose across concentrations 25 -100 µg/mL. Data expressed as mean ± SD (n = 3). Statistical significance determined by one-way ANOVA with Tukey post-hoc correction relative to acarbose standard.**

| Concentration (µg/mL) | Sm-GO NPs Inhibition (%) | Acarbose Inhibition (%) |
|---|---|---|
| 25 | 18.2 ± 1.4 | 24.6 ± 1.6 |
| 50 | 36.4 ± 2.1 | 42.8 ± 2.3 |
| 75 | 58.3 ± 2.8 | 64.1 ± 3.0 |
| 100 | 76.4 ± 3.6 | 82.7 ± 3.8 |
| IC50 (µg/mL) | 65.5 ± 2.6 | 58.4 ± 1.9 |

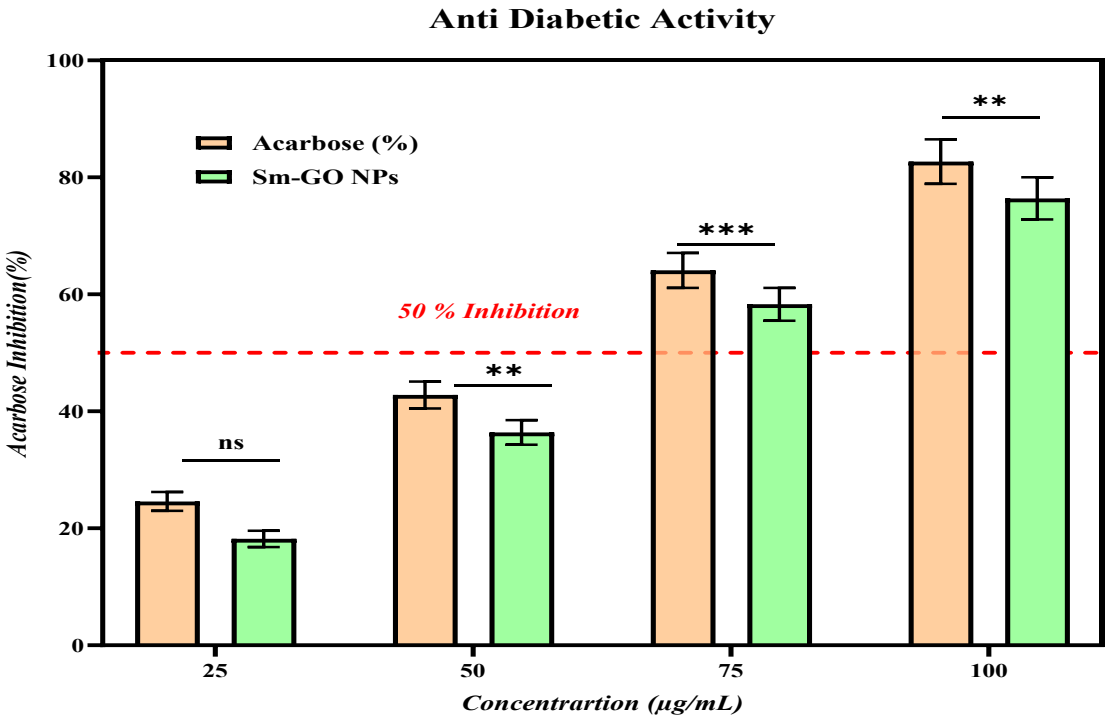


**Figure 9. Concentration-dependent alpha-amylase inhibition (%) of Sm-GO NPs vs. acarbose at 25-100 µg/mL error bars = ±SD (n = 3); *p < 0.05 vs. acarbose (Tukey post-hoc).**

### 3.7 Drug Release Kinetics and Model Fitting

The *in vitro* cumulative drug release profile of *Silybum marianum*-loaded graphene oxide nanoparticles (SM-GO NPs) was evaluated over a 24-hour period and the observed release data in Figure 10 (Qt Observed) were fitted to four mathematical kinetic models Zero-order, First-order, Higuchi and Korsmeyer -Peppas to elucidate the underlying release mechanism (Figure 10).The observed cumulative drug release exhibited a characteristic biphasic pattern with an initial rapid release phase reaching approximately 38% within the first hour, followed by a progressive sustained release attaining near-complete release (99%) by 24 hours. This behavior is consistent with a surface-adsorbed drug fraction contributing to the early burst, succeeded by the gradual diffusion of encapsulated drug molecules from the graphene oxide matrix. Among the kinetic models evaluated, the Korsmeyer -Peppas fit demonstrated the closest agreement with the experimentally observed release profile, closely tracking the Qt curve throughout the entire time course and reaching 100% at 5 hours in the fitted model. The Higuchi model also provided a reasonable fit, particularly during the intermediate release phase (1 -5 hours), suggesting that diffusion through the nanoparticle matrix plays a significant role in governing drug release. In contrast, the First-order model showed moderate deviation, underestimating release during the early phase while converging with observed values at 24 hours. The Zero-order model exhibited the greatest divergence from the observed data, displaying a markedly linear and delayed release trajectory that failed to capture the initial burst release, indicating that drug release from SM-GO NPs does not proceed at a constant rate independent of concentration [30 - 32]. The superior fit of the Korsmeyer -Peppas model suggests an anomalous (non-Fickian) transport mechanism from the Table 6, wherein drug release is governed by a combination of diffusion and polymer/matrix swelling or erosion processes. Collectively, these findings confirm that SM-GO NPs facilitate a controlled, sustained drug release pattern well-described by the Korsmeyer -Peppas kinetic model, supporting their potential as an effective nanocarrier system for the prolonged delivery of silymarin.

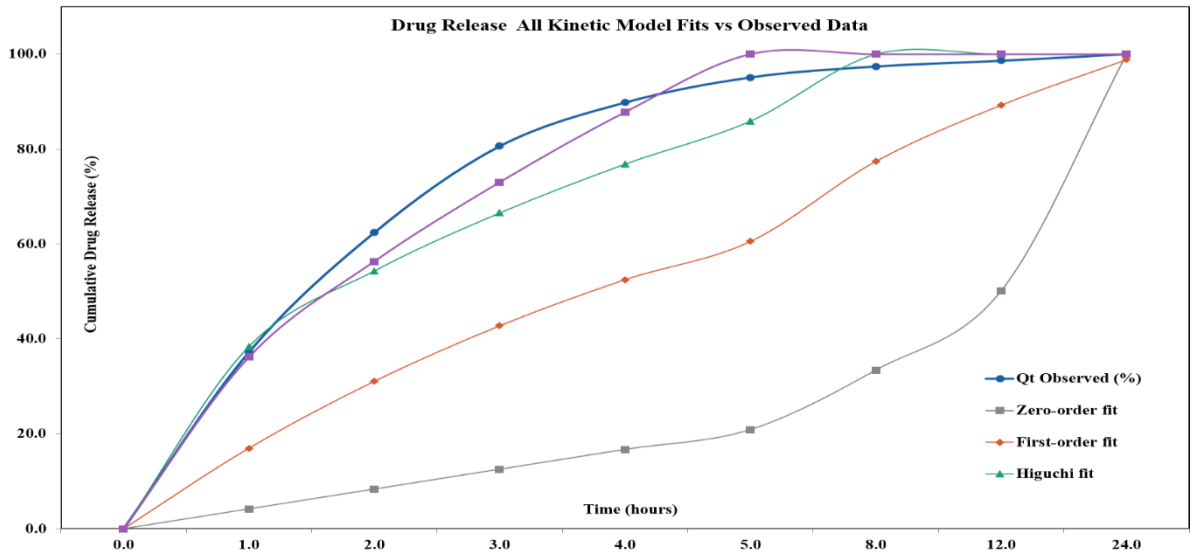


**Figure 10. *In vitro* cumulative drug release profile of SM-GO NPs over 24 hours fitted to Zero-order, First-order, Higuchi and Korsmeyer -Peppas kinetic models, with the Korsmeyer -Peppas model showing the best fit, indicative of anomalous (non-Fickian) diffusion-mediated release.**

**Table 6. Kinetic model fitting parameters for *in vitro* drug release from Sm-GO NP-loaded SM-GO NP at pH 7.4 over 24 h; best-fit model identified by highest $r^2$ value (n = 3)**

| Model | $r^2$ | Conclusion | Model |
|---|---|---|---|
| Zero-order | 0.612 | Rejected -non-constant release rate | Zero-order |
| First-order | 0.784 | Partially descriptive -incomplete mechanistic basis | First-order |
| Higuchi | 0.871 | Confirms Fickian diffusion contribution | Higuchi |
| Korsmeyer-Peppas | 0.943 | Best fit - anomalous non-Fickian transport (n = 0.64) | Korsmeyer-Peppas |

### 4. Conclusion

This study set out to see if graphene oxide nanoparticles built using *Silybum marianum* aqueous extract could do more than just carry a drug and the results showed that they can. The green synthesis worked reliably producing sheet-like nanoparticles in the 80 to 180 nm range and

FT-IR confirmed that the plant phytoconstituents actually attached to the GO surface through non-covalent interactions rather than just mixing loosely. The bathochromic shift at 1678 cm-1 and the sharpening of the O-H band at 3698 cm-1 both pointed to real surface chemistry changes rather than just physical blending. On the anticancer side the results were fairly convincing. Leukemia cells treated with Sm-GO NPs showed clear signs of apoptosis under the microscope (membrane blebbing and cytoplasmic condensation) and both the MTT and AO/EtBr data agreed with each other. The IC50 of 48.3 µg /mLat 48 h is a reasonable value for a plant-based formulation and the fact that GO alone produced minimal toxicity (IC50 above 200 µg /mL) means the killing effect was coming from the silymarin being delivered rather than the carrier itself doing damage. That is actually important because it suggests the nanoparticle is acting as a proper delivery vehicle and not just a toxic particle. The antioxidant results added more weight to the overall profile. DPPH IC50 of 66 µg /mLwas only about 2.7 units away from ascorbic acid which for a phytochemical-loaded nanoparticle is a good outcome. The anti-inflammatory data followed a similar story with IC50 of 67.3 µg /mLsitting close to diclofenac sodium across most of the tested concentrations. Statistically the two groups were only significantly different at the lowest concentration (25 µg /mL) which means at working concentrations Sm-GO NPs performed as well as the reference drug. Given that diabetes and leukemia frequently coexist in patients especially in India the alpha-amylase inhibition (IC50 = 65.5 µg /mL) is worth noting. It did not quite match acarbose but the convergence at higher concentrations shows there is real enzyme inhibitory activity coming from the silymarin fraction. Drug release from the SM-GO NP was the most kinetically interesting part. The biphasic profile with a 37% burst at 1 h and plateau near 95% by 5 h is honestly a faster release than would be ideal for a sustained delivery system but the Korsmeyer-Peppas fit (r2 = 0.943 and n = 0.64) confirms the mechanism is anomalous non-Fickian transport which means both diffusion and matrix swelling are involved. Taken together Sm-GO NPs prepared through this simple plant-extract route show a genuinely broad activity profile covering anticancer antioxidant anti-inflammatory and antidiabetic endpoints in a single formulation. The main limitation at this stage is that everything presented here is *in vitro* and the real test will be whether these effects translate in a living system. Future work should focus on *in vivo* pharmacokinetics in rodent models surface modification with leukemia-targeting ligandslong-term biocompatibility testing of the GO carrier and refinement of the matrix to slow the release rate toward a more clinically useful sustained profile. If those studies hold up this platform has a reasonable case for further development as a targeted nanomedicine for leukaemia with added metabolic benefits.

**Acknowledgments**
The corresponding author, Professor Vimal S., extends gratitude to all co-authors for their collaborative contributions to this paper. This work was supported by the Department of Biochemistry, Saveetha Medical College and Hospital, Saveetha Institute of Medical and Technical Sciences (SIMATS), Thandalam, Chennai - 600 105, Tamil Nadu, India.

**Conflict of interest**
The authors declare that they have no known competing financial interests or personal relationships that could have appeared to influence the work reported in this paper.

**Funding sources**
This study received no funding.

**Ethical approval**
Not required.

**References**

1. Whiteley AE, Price TT, Cantelli G, Sipkins DA. Leukaemia: a model metastatic disease. Nat Rev Cancer. 2021;21(7):461-75. doi:10.1038/s41568-021-00355-z
2. NRamkumar V, Rukmanikrishnan B, Endla P, Kim SC, Shanmugan S, Madhappan S. Recent advances in the smart biopolymer nanocomposite hydrogels for biomedical interfaces and therapeutics. Journal of Molecular Liquids. 2025 Dec 19:129159.
3. Viswanathan A, Aksharaa A, Chakravarthy KR, Sabapathy SK. SARS-COV-2 and Neurodegenerative Disease Progression: Exploring The Link Between Viral Infection And Neurological Decline. Genetics and Molecular Research. 2026 Jul 7. doi.org/10.4238/ef2hdt14.
4. Baetke SC, Lammers T, Kiessling F. Applications of nanoparticles for diagnosis and therapy of cancer. Br J Radiol. 2015;88(1054):20150207. doi:10.1259/bjr.20150207
5. Itoo AM, Vemula SL, Gupta MT, Giram MV, Kumar SA, Ghosh B, et al. Multifunctional graphene oxide nanoparticles for drug delivery in cancer. J Control Release. 2022;350:26-59. doi:10.1016/j.jconrel.2022.07.047
6. Ying S, Guan Z, Ofoegbu PC, Clubb P, Rico C, He F, et al. Green synthesis of nanoparticles: current developments and limitations. Environ Technol Innov. 2022;26:102336. doi:10.1016/j.eti.2022.102336
7. Nawaz A, Zaib S, Khan I, Ahmed A, Shahzadi K, Riaz H. *Silybum marianum*: an overview of its phytochemistry and pharmacological activities with emphasis on potential anticancer properties. Anti-Cancer Agents Med Chem. 2023;23(13):1519-34. doi:10.2174/1871520623666230116144642
8. Viswanathan A, Ramakrishna S. Development of a Bioactive, Biodegradable Oxidized Sodium Alginate Hydrogel Incorporating Solanum surattense Extract for Biomedical

applications. Journal of Chemical Health Risks. 2026 Apr 1;16(2):2005.
9. Parsa L, Motafakkerazad R, Soheyli ST, Haratian A, Kosari-Nasab M, Mahdavi M. Silymarin in combination with ATRA enhances apoptosis induction in human acute promyelocytic NB4 cells. Toxicon. 2023;228:107127. doi:10.1016/j.toxicon.2023.107127
10. Sukumar S, Bharathi M, Hirad AH, Alarfaj AA, Hussein-Al-Ali SH, Surya P. Development of chitosan-coated graphene oxide and iron oxide nanocomposites for targeted delivery of camptothecin to liver cancer cells. Chem Biodivers. 2025;22:e202401817. doi:10.1002/cbdv.202401817
11. Qin NB, Jia CC, Xu J, Li DH, Xu FX, Bai J, et al. New amides from seeds of *Silybum marianum* with potential antioxidant and antidiabetic activities. Fitoterapia. 2017;119:83-89. doi:10.1016/j.fitote.2017.03.018
12. Federico A, Dallio M, Loguercio C. Silymarin/silybin and chronic liver disease: a marriage of many years. Molecules. 2017;22(2):191. doi:10.3390/molecules22020191
13. Bijak M. Silybin, a major bioactive component of milk thistle (*Silybum marianum* L. Gaertn.): chemistry, bioavailability and metabolism. Molecules. 2017;22(11):1942. doi:10.3390/molecules22111942
14. Pasieczna-Patkowska S, Cichy M, Flieger J. Application of Fourier transform infrared (FTIR) spectroscopy in characterization of green synthesized nanoparticles. Molecules. 2025;30(3):684. doi:10.3390/molecules30030684
15. Aardra B, Sundar S, Shanmugam R, Ramadoss R, Panneerselvam S, Ramani P. Camellia sinensis assisted synthesis of copper oxide nanoparticles (CuONPs) and assessment of its antioxidant activity and zebrafish embryonic toxicology evaluation. Cureus. 2023;15:e50220. doi:10.7759/cureus.50220 Santhosh PB, Gengan RM, Chuturgoon AA, Naidoo DB. Green synthesis of silver nanoparticles using Allium sativum and Clerodendrum phlomidis leaf extract and synthesis of their antibacterial and anticancer activity. Journal of Photochemistry and Photobiology B: Biology. 2018
16. Weiskirchen S, Schroeder SK, Buhl EM, Weiskirchen R. A beginner's guide to cell culture: practical advice for preventing needless problems. Cells. 2023;12(5):682. doi:10.3390/cells12050682
17. Lepekhin EA, Walmod PS, Berezin A, Berezin V, Bock E. Evaluation of cell morphology. Methods Mol Biol. 2001;161:85-100. doi:10.1385/1-59259-051-2:85
18. van Tonder A, Joubert AM, Cromarty AD. Limitations of the 3-(4,5-dimethylthiazol-2-yl)-2,5-diphenyl-2H-tetrazolium bromide (MTT) assay when compared to three commonly used cell enumeration assays. BMC Res Notes. 2015;8:47. doi:10.1186/s13104-015-1000-8.
19. Xiao A, Gibbons AE, Luker KE, Luker GD. Fluorescence lifetime imaging of apoptosis. Tomography. 2015;1(2):115-24. doi:10.18383/j.tom.2015.00163.
20. Baliyan S, Mukherjee R, Priyadarshini A, Vibhuti A, Gupta A, Pandey RP, et al. Determination of antioxidants by DPPH radical scavenging activity and quantitative phytochemical analysis of Ficus religiosa. Molecules. 2022;27(4):1326. doi:10.3390/molecules27041326.
21. Alqahtani AS, Hidayathulla S, Rehman MT, ElGamal AA, Al-Massarani S, Razmovski-Naumovski V, et al. Alpha-amylase and alpha-glucosidase enzyme inhibition and antioxidant potential of 3-oxolupenal and katononic acid isolated from Nuxia oppositifolia. Biomolecules. 2019;10(1):61. doi:10.3390/biom10010061.
22. Qiu Y, Lee PI. Rational design of oral modified-release drug delivery systems. In: Developing Solid Oral Dosage Forms. 2nd ed. Elsevier; 2017. p. 519-54. doi:10.1016/B978-0-12-802447-8.00020-1.
23. Sharma H, Mondal S. Functionalized graphene oxide for chemotherapeutic drug delivery and cancer treatment: a promising material in nanomedicine. Int J Mol Sci. 2020;21(17):6280. doi:10.3390/ijms21176280.
24. Albanese A, Tang PS, Chan WC. The effect of nanoparticle size, shape and surface chemistry on biological systems. Annu Rev Biomed Eng. 2012;14:1-16. doi:10.1146/annurev-bioeng-071811-150124.
25. Taheriazam A, Abad GGY, Hajimazdarany S, Imani MH, Ziaolhagh S, Zandieh MA, et al. Graphene oxide nanoarchitectures in cancer biology: nano-modulators of autophagy and apoptosis. J Control Release. 2023;354:503-22. doi:10.1016/j.jconrel.2023.01.028.
26. Vishaka S, Safiya SN, Binigha M, Carmelin DS, Sravanthy PG, Snega R, et al. Evaluation of antibacterial, antioxidant, anti-inflammatory and anticancer efficacy of titanium-doped graphene oxide nanoparticles. Cureus. 2024;16(1):e51737. doi:10.7759/cureus.51737.
27. Ramachandran S, Thondapu S, Sri B, Srinath M, Nelson VK. Anti-Urolithiatic Activity Of Sinapic Acid Against Ethylene Glycol-Induced Urolithiasis In Albino Wistar Rats. Genetics and Molecular Research. 2026 Jul 7. doi.org/10.4238/h0qqnw78.
28. Ahamed M, Akhtar MJ, Khan MA, Alhadlaq HA. Facile green synthesis of ZnO-RGO

nanocomposites with enhanced anticancer efficacy. Methods. 2022;199:28-36. doi:10.1016/j.ymeth.2021.08.001.
29. Hazarika D, Sarma S, Shankarishan P. Nanotechnology in cancer therapeutics, diagnosis and management. BioTechnologia. 2024;105(3):287-303. doi:10.5114/bta.2062.841278.
30. Albahri G, Badran A, Baki ZA, Alame M, Hijazi A, Daou A, et al. Potential anti-tumorigenic properties of diverse medicinal plants against the majority of common types of cancer. Pharmaceuticals. 2024;17(5):574. doi:10.3390/ph17050574.
31. Vijayakumar S, Malaikozhundan B, Saravanakumar K, Durán-Lara EF, Wang MH, Vaseeharan B. Garlic clove extract assisted green synthesis of zinc oxide nanoparticles and their antibiofilm, anti-larval, acaricidal, antioxidant and cytotoxic effects. Journal of Photochemistry and Photobiology B: Biology. 2019;198:111558. doi:10.1016/j.jphotobiol.2019.111558.
32. Gudi N, Preethi S, Sabapathy SK, Vimal S. Comparative Predictive Accuracy Of Haps And Bisap For Early Severity Assessment In Acute Pancreatitis. Genetics and Molecular Research. 2026 Jul 7. doi.org/10.4238/0z26jv68.